CrossMark
click for updates

# Titanium oxo-clusters derivatized from the $Ti_{10}O_{12}(cat)_8(py)_8$ complex: structural investigation and spectroscopic studies of light absorption†

Clément Chaumont,[a] Alain Chaumont,[a] Nathalie Kyritsakas,[b] Pierre Mobian*[a] and Marc Henry[a]

A series of deep-red colored nano-sized titanium oxo-clusters bearing catecholato ligands is reported. These architectures are produced *via* post-synthetic modification of the $Ti_{10}O_{12}(cat)_8(py)_8$ (cat = catecholato, py = pyridine) complex through quantitative substitution of labile pyridine ligands by three substituted pyridines (pico, 4-Phpy and pyrald). The crystal structure analysis reveals a common $Ti_{10}O_{12}(cat)_8$ backbone for the three isolated molecular architectures. Partial charge analysis indicates two types of titanium atoms within these complexes with one resembling titanium(IV) found in $TiO_2$. These complexes strongly absorb visible light in solution ($\lambda_{max}$ = 411 nm, $\varepsilon$ = 10 800 for $Ti_{10}O_{12}(cat)_8(py)_8$ in $CHCl_3$) and in the solid-state. The band gaps estimated from the reflectance spectra are between 1.85 eV and 1.97 eV. The present work also details the HOMO and LUMO representations obtained *via* DFT calculation for $Ti_{10}O_{12}(cat)_8(py)_8$ and a virtual $Ti_{10}O_{12}(cat)_8$ complex as well as the DOS (density of states) plots calculated for those structures. This computational study highlights an impact of the pyridine ligand on the DOS plots.

[a]*Laboratoire de Chimie Moléculaire de l'Etat Solide, UMR UDS-CNRS 7140, Université de Strasbourg, Institut Le Bel, 4, rue Blaise Pascal, F-67000 Strasbourg, France. E-mail: mobian@unistra.fr*
[b]*Laboratoire de Tectonique Moléculaire, UMR UDS-CNRS 7140, icFRC, University of Strasbourg, Institut Le Bel, 4, rue Blaise Pascal, F-67000 Strasbourg, France*
†Electronic supplementary information (ESI) available. CCDC 1413510–1413512. For ESI and crystallographic data in CIF or other electronic format see DOI: 10.1039/c6dt00632a

## Introduction
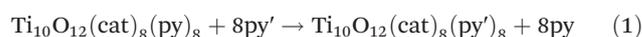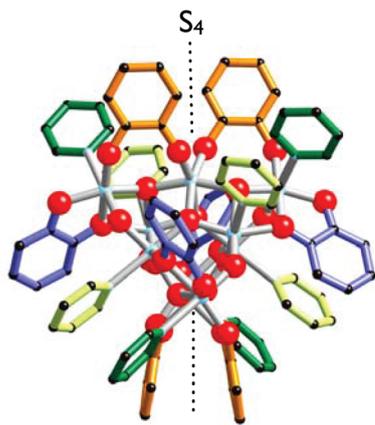
Titanium dioxide ($TiO_2$) is a cheap non-toxic semiconductor, which elicits a major interest for applications in photocatalytic water splitting,[1] photocatalytic degradation of pollutants[2] or solar energy conversion.[3] However, $TiO_2$ does not absorb the visible light of solar radiation due to its high band gap (3.2 eV). Therefore, to develop more practical $TiO_2$-based photo-active materials, research studies are actually focused on materials that can absorb light in the visible domain.

Titanium oxo-clusters[4] are a fascinating class of compounds that are intensively investigated as models of bulk $TiO_2$. In particular, in the context of visible-light-active $TiO_2$-based materials, the synthesis and study of the optical properties of polyoxotitanium complexes absorbing light in the visible region represent an intensive field of research. Mainly, two classes of polyoxotitanate architectures are developed. The broad family of metal-doped polyoxotitanium complexes are

viewed as ligand-stabilized molecular fragments of metal-doped $TiO_2$, and several metal ions, including Fe(II),[5] Ga(III),[6] Co(II),[7] Mn(II),[8] lanthanide ions,[9] and alkali metal ions,[10] have been incorporated in these structures. The band gap of these compounds has shown to be reduced in comparison with classical oxo-titanium clusters. Another class of titanium oxo-clusters concerns nanoclusters decorated with sensitizers.[11] High nuclearity clusters bearing catecholato[10,12] or 2,2′-biphenolato[11,13] ligands have been reported as the $Ti–O_{(phenolato)}$ bond is known to absorb in the visible domain, due to the charge transfer between the lone pair of oxygen atoms and the empty 3d-orbitals of the Ti(IV) ions.[14]

Very recently, we have reported the structural characterization of a high nuclearity catecholato-based Ti(IV) architecture bearing pyridine ligands. This complex formulated as $Ti_{10}O_{12}(cat)_8(py)_8$ (cat = catecholato, py = pyridine) displays a $S_4$ symmetry as shown in the crystal structure in Fig. 1.[15] Importantly, the unusual behaviour of this complex in solution was studied by various NMR techniques highlighting the labile behaviour of the pyridine ligands.

In this manuscript, we report some architectures derived from the $Ti_{10}O_{12}(cat)_8(py)_8$ complex. These nanosized clusters incorporating various substituted pyridines (py′) were obtained by exploiting the lability of the pyridine ligands decorating the $Ti_{10}O_{12}(cat)_8$ core of the complex as proposed in eqn (1):

$$Ti_{10}O_{12}(cat)_8(py)_8 + 8py' \rightarrow Ti_{10}O_{12}(cat)_8(py')_8 + 8py \quad (1)$$

**Fig. 1** View of the molecular structure of $Ti_{10}O_{12}(cat)_8(py)_8$ evidencing the $S_4$-symmetry of the complex. The two inequivalent catecholato ligands are colored differently (in orange and light purple). The pyridine ligands are displayed in two colors depending on their localizations in the complex. The pyridine ligands colored in light green (named as py (int.)) correspond to ligands sandwiched between a catecholato ligand (in purple) and a second pyridine ligand colored in dark green (named as py(ext.)). The titanium atoms and the oxygen atoms are in blue and red respectively. Hydrogen atoms are omitted for clarity.
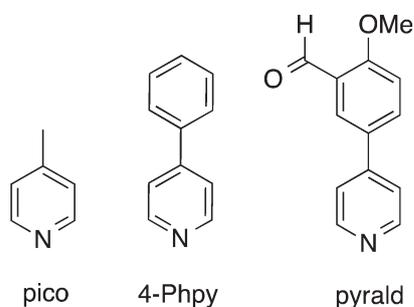


**Fig. 2** Pyridine derivatives (py') employed in the study.

The crystalline structures of new $Ti_{10}O_{12}(cat)_8$-based complexes bearing substituted pyridines are reported and discussed related to the initial $Ti_{10}O_{12}(cat)_8(py)_8$ complex. The substituted pyridine ligands incorporated in these new nanosized architectures are 4-picoline (pico), 4-phenylpyridine (Phpy) and 2-methoxy-5-(pyridin-4-yl)-benzaldehyde (pyrald) (see Fig. 2).

In order to compare these oxo-clusters to $TiO_2$ phases, the partial charge distribution was determined for these species. In parallel, we present DFT calculations to determine the HOMO–LUMO gaps for these complexes. These data are correlated with the experimental spectroscopic data recorded for this series of red-colored polyoxotitanium complexes.

## $Ti_{10}O_{12}(cat)_8(py)_8$ in solution: NMR investigation

Before studying the substitution of pyridine ligands linked to the $Ti_{10}O_{12}(cat)_8$ core of the complex, full characterization of the complex in solution is mandatory. At room temperature, the DOSY experiment run in $CDCl_3$ clearly suggests the deco-ordination of the pyridine ligands.[14] Furthermore, three large signals at $\delta$ = 8.40, 7.53 and 7.10 ppm attributed to pyridine highlight an exchange process as shown by the $Ti_{10}O_{12}$-$(cat)_8(py)_8$ spectrum at room temperature (Fig. 3c). At low temperature (see Fig. 3b), the ${}^1H$ NMR spectrum changes drastically since sharp signals are predominant. However, due to the complexity of the spectrum, the distinction between signals belonging to the catecholato and pyridine ligands is rather difficult. Thus, the spectrum at low temperature of a new complex bearing deuterated pyridine ligands was recorded. This complex formulated as $Ti_{10}O_{12}(cat)_8(py-d_5)_8$ is prepared like $Ti_{10}O_{12}(cat)_8(py)_8$. At low temperature, the ${}^1H$ NMR spectrum of $Ti_{10}O_{12}(cat)_8(py-d_5)_8$ appears to be much simpler than the nondeuterated complex since only signals attributed to the catecholato ligands are observed (Fig. 3a). Now, the assignment of
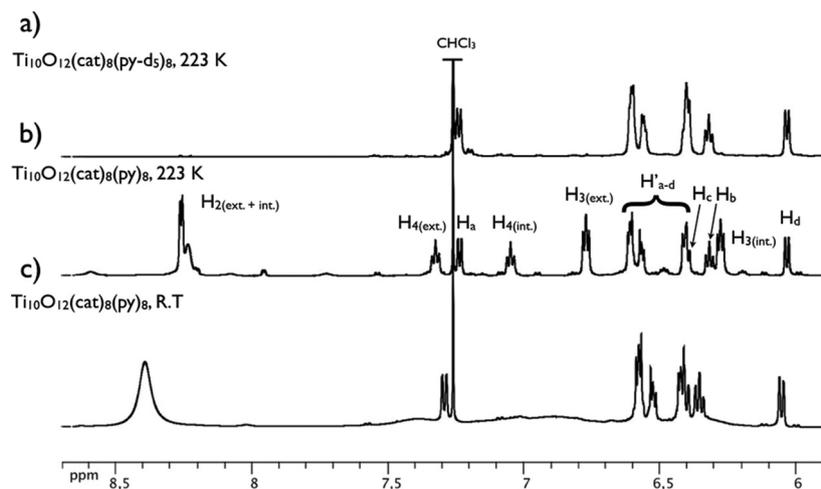


**Fig. 3** ${}^1H$ NMR spectra of $Ti_{10}O_{12}(cat)_8(py)_8$ at room temperature, of $Ti_{10}O_{12}(cat)_8(py)_8$ at 223 K and $Ti_{10}O_{12}(cat)_8(py-d_5)_8$ at 223 K in $CDCl_3$ (aromatic region).

the pyridine ligand signals in spectrum 1b becomes straightforward. The presence of two sets of pyridine proton resonances ($\delta$ = 7.32 ppm, 6.77 ppm and $\delta$ = 7.05 ppm, 6.27 ppm) for protons $H_3$ and $H_4$ (Fig. 4) is in full accord with the two types of pyridine ligands observed in the crystal structure (named py(int.) and py(ext.) in Fig. 1 legend). As in the structure, four py(int.) ligands are sandwiched between catecholato and py(ext.) ligands, the assignment of the upfield shifted pyridine proton resonances to py(int.) protons is proposed ($\delta$ = 7.05 ppm and 6.27 ppm). Consequently, the signals at $\delta$ = 7.32 ppm and 6.77 ppm correspond to the NMR signature of $H_4$ and $H_3$ of py(ext.) respectively. The COSY spectrum permits also the partial assignment of the signals of the catecholato ligands. The signal at $\delta$ = 6.03 ppm is abnormally upfield shifted in comparison with the other catecholato proton signals. A close examination of the $Ti_{10}O_{12}(cat)_8(py)_8$ crystal structure provides evidence to the environment of the $H_d$ protons (the labels of the catecholato protons are given in Fig. 4). These protons, belonging to the bridging catecholato ligands are localized in the shielding cone of a second bridging catecholato ligand. The distance measured between these protons and the nearest catecholato ring centroids is estimated to be 3.7 Å. This nicely explains the chemical shift observed for this signal. Next, according to the correlation observed by COSY, the assignment of the resonances of all protons belonging to the bridging catecholato ligands is made. Finally, the rest of the catecholato proton resonances (from $\delta$ = 6.7 to 6.4 ppm) are attributed to protons of the singly bridging catecholato ligands.

## Complex synthesis and crystal structure description

After the $Ti_{10}O_{12}(cat)_8(py)_8$ low-temperature $^1H$ NMR spectrum assignment, the pyridine ligand substitution study was undertaken as proposed in eqn (1). The post-synthetic modification of titanium-oxo clusters represents a very challenging task since a reorganization of the titanium oxo backbone after the substitution reaction is generally observed.[16] Only a few examples of a post-synthetic cluster modification without any alteration of the inorganic core of the initial Ti(IV) oxo-cluster are reported in the literature.[17]

Many different substituted pyridine compounds have been tested with very limited success concerning the isolation of the desired products as crystalline solids. The tested pyridine derivatives include lutidine derivatives, pyridine rings functionalized with electron donating or withdrawing groups or pyridine rings substituted with sterically hindered groups. However, when the reactions were conducted with the pico, 4-Phpy and pyrald compounds, after the diffusion of diethylether, crystals of the targeted compounds were isolated in quantitative yields. It is worth noticing that the pico and 4-Phpy compounds are commercially available products whereas the pyrald derivative is a key intermediate for the preparation of several molecules.[18] These new complexes were characterized by NMR spectroscopy, infrared spectroscopy and elemental analysis. The $S_4$ symmetry of these titanium oxo-clusters in solution was confirmed by $^{13}C$ NMR since four resonances attributed to $\underline{C}-O_{(catecholato)}$ are observed in the spectra of the complexes dissolved in $CDCl_3$.

Single crystals of the complexes were obtained by dissolving the $Ti_{10}O_{12}(cat)_8(py)_8$ complex in chloroform with a slight excess of the substituted pyridines. Dark red single crystals suitable for X-ray diffraction analysis were obtained for the pico, 4-Phpy and pyrald compounds by slow diffusion of diethylether in a few days period. The crystal structure resolution reveals that compounds obtained with 4-Phpy and pyrald crystallize in the $I4_1/a$ space group whereas the third compound crystallizes in the $P\bar{1}$ space group. In each crystalline network, the complex co-crystallizes with chloroform molecules. The molecular structures of these complexes are shown in Fig. 5(a–c).

The three complexes are nanosized objects with molecular volumes estimated to be 1370 Å$^3$, 2110 Å$^3$ and 2464 Å$^3$ for $Ti_{10}O_{12}(cat)_8(pico)_8$, $Ti_{10}O_{12}(cat)_8(4\text{-Phpy})_8$ and $Ti_{10}O_{12}(cat)_8(pyrald)_8$ respectively. The structures reveal that the resulting complexes display $Ti_{10}O_{12}(cat)_8$ backbones identical to the one observed for the $Ti_{10}O_{12}(cat)_8(py)_8$ precursor. The overviews of the superposed $Ti_{10}O_{12}(cat)_8(py)_8$ structure with the $Ti_{10}O_{12}(cat)_8(pico)_8$, $Ti_{10}O_{12}(cat)_8(4\text{-Phpy})_8$ and $Ti_{10}O_{12}(cat)_8(pyrald)_8$ structures respectively highlight these structural similarities (Fig. 6).
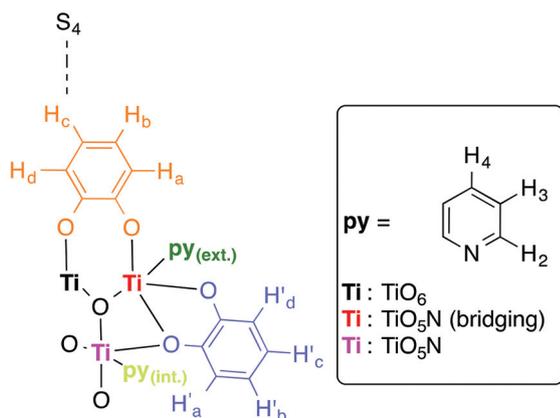


**Fig. 4** Representation of the ligands of $Ti_{10}O_{12}(cat)_8(py)_8$ with labelled protons. For clarity, the complex is only partially represented. The protons labelled as $H_a$, $H_b$, $H_c$ and $H_d$ belong to the catecholato ligands adopting a singly bridging $\mu^2$-(O,O') mode (these ligands are colored in orange in Fig. 1). The protons labelled as $H'_a$, $H'_b$, $H'_c$ and $H'_d$ belong to the second type of catecholato ligand colored in purple in the structure (these ligands display a singly bridging chelate $\mu^2$-(O,O',O') mode (Fig. 1)). The pyridine protons are labelled as $H_3$, $H_4$ and $H_5$ ext. or int. (ext. and int. referring to the localization of these ligands in the complex). H(int.) concerns the protons of the pyridine ring py(int.) (colored in light green in the structure (Fig. 1)). H(ext.) refers to the protons of the pyridine rings, py(ext.) that decorate the external part of the complex and colored in dark green in the structure (Fig. 1). Titanium ions in black, red and pink refers to $TiO_6$, $TiO_5N$ (bridging) and $TiO_5N$ respectively.
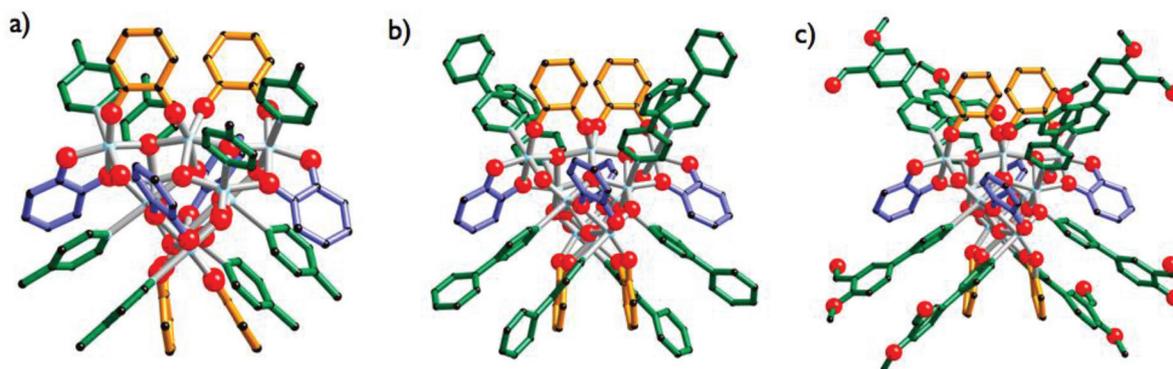
**Fig. 5** (a) Molecular structure of $Ti_{10}O_{12}(cat)_8(pico)_8$. (b) Molecular structure of $Ti_{10}O_{12}(cat)_8(4\text{-Phpy})_8$. (c) Molecular structure of $Ti_{10}O_{12}(cat)_8$-$(pyrald)_8$. In these structures, the two inequivalent catecholato ligands are differently colored (in orange and light purple). The pyridine ligands are colored in green. The titanium atoms and the oxygen atoms are in blue and red respectively. This inorganic core is composed of ten titanium atoms, eight $\mu^3$-oxo bridges (two inequivalent $\mu^3$-oxo bridges are present), and four $\mu^2$-oxo bridges; the other oxygen atoms belong to the catecholato ligands.
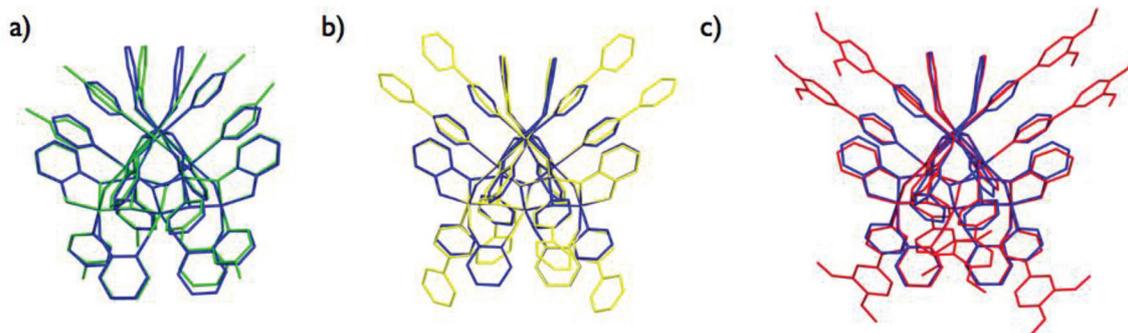


**Fig. 6** (a) Overlay of the $Ti_{10}O_{12}(cat)_8(py)_8$ complex (blue) with the $Ti_{10}O_{12}(cat)_8(pico)_8$ complex (green). (b) Overlay of the $Ti_{10}O_{12}(cat)_8(py)_8$ complex (blue) with the $Ti_{10}O_{12}(cat)_8(4\text{-Phpy})_8$ complex (yellow). (c) Overlay of the $Ti_{10}O_{12}(cat)_8(py)_8$ complex (blue) with the $Ti_{10}O_{12}(cat)_8(pyrald)_8$ complex (red).

For the new complexes no residual pyridine ligand is found and eight substituted pyridine ligands (py′) are linked to the inorganic core of the complexes leading to clusters displaying the respective $Ti_{10}O_{12}(cat)_8(pico)_8$, $Ti_{10}O_{12}(cat)_8(4\text{-Phpy})_8$ and $Ti_{10}O_{12}(cat)_8(pyrald)_8$ formulae. In these structures, as for the $Ti_{10}O_{12}(cat)_8(py)_8$ complex, two types of rarely observed coordination modes for the catecholato ligands are noticed. The purple colored catecholato ligands in Fig. 5 represent the four ligands adopting a singly bridging chelate $\mu^2$-(O,O′,O′) mode, whereas the singly bridging $\mu^2$-(O,O′) mode involves the four catecholato ligands colored in orange. The inorganic core of the complexes is formed by four $\mu^2$-oxo and eight $\mu^3$-oxo bridging ligands with two types of inequivalent $TiO_5N$ subunits and one type of $TiO_6$ polyhedron. It is worth noticing that $Ti_{10}O_{12}(cat)_8(4\text{-Phpy})_8$ and $Ti_{10}O_{12}(cat)_8(pyrald)_8$ adopt a perfect $S_4$ symmetry whereas $Ti_{10}O_{12}(cat)_8(pico)_8$ displays a pseudo $S_4$ symmetry. The dissymmetry found in $Ti_{10}O_{12}(cat)_8$-$(pico)_8$ arises from metrical factors. For instance, the distances separating two titanium atoms coordinated with the same catecholato ligand in the bridging $\mu^2$-(O,O′) mode are different in $Ti_{10}O_{12}(cat)_8(pico)_8$ ($Ti_3\cdots Ti_6 = 3.513$ Å, $Ti_5\cdots Ti_6 = 3.504$ Å).

The $S_4$ symmetry of $Ti_{10}O_{12}(cat)_8(pico)_8$ in solution is proved by $^{13}C$ NMR spectroscopy, as four resonances attributed to $\underline{C}$–$O_{(catecholato)}$ at $\delta = 159.4$ ppm, 157.5 ppm, 155.9 ppm, and 154.1 ppm are observed. The same observation in solution is made for the $Ti_{10}O_{12}(cat)_8(4\text{-Phpy})_8$ complex, whereas NMR analysis in solution is impossible to handle for $Ti_{10}O_{12}(cat)_8$-$(pyrald)_8$ due to the insolubility of the complex.

Concerning the metrical description of the complexes, the Ti$\cdots$N bond distances are similar to those found in $Ti_{10}O_{12}$-$(cat)_8(py)_8$ (the Ti–N bond distances are given in Table SI†). Clearly, the lengths of the Ti–N bonds are not affected by the nature of the substituents decorating the pyridine rings.

## Partial charge analysis

The partial charge calculation for the four complexes was performed with the PACHA software.[19] The charges found in these complexes for the oxygen atoms are unexceptional. These charges are listed in Table 1. The charges of the oxygen atoms belonging to the catecholato ligands range from

**Table 1** Charges computed for the oxygen atoms in $Ti_{10}O_{12}(cat)_8(py)_8$, $Ti_{10}O_{12}(cat)_8(4\text{-Phpy})_8$, $Ti_{10}O_{12}(cat)_8(pico)_8$ and $Ti_{10}O_{12}(cat)_8(pyrald)_8$

| | $q(O(cat))$ | $q(\mu^2\text{-}O(cat))$ | $q(\mu^2\text{-}O)$ | $q(\mu^3\text{-}O)$ |
|---|---|---|---|---|
| $Ti_{10}O_{12}(cat)_8(py)_8$ | O3 = −0.55 <br> O4 = −0.52 <br> O2 = −0.52 | O1 = −0.61 | O7 = −0.77 | O5 = −0.86 <br> O6 = −0.85 |
| $Ti_{10}O_{12}(cat)_8(4\text{-Phpy})_8$ | O4 = −0.55 <br> O5 = −0.52 <br> O6 = −0.50 | O7 = −0.61 | O3 = −0.76 | O1 = −0.86 <br> O2 = −0.85 |
| $Ti_{10}O_{12}(cat)_8(pico)_8$ | O28 = −0.55 <br> O21 = −0.55 <br> O19 = −0.54 <br> O15 = −0.54 <br> O22 = −0.53 <br> O27 = −0.53 <br> O20 = −0.52 <br> O16 = −0.51 <br> O26 = −0.51 <br> O23 = −0.50 <br> O14 = −0.50 <br> O18 = −0.50 | O13 = −0.61 <br> O17 = −0.61 <br> O24 = −0.60 <br> O25 = −0.60 | O6 = −0.77 <br> O2 = −0.77 <br> O12 = −0.77 <br> O5 = −0.77 | O8 = −0.87 <br> O11 = −0.87 <br> O4 = −0.86 <br> O1 = −0.86 <br> O9 = −0.86 <br> O10 = −0.86 <br> O7 = −0.85 <br> O3 = −0.85 |
| $Ti_{10}O_{12}(cat)_8(pyrald)_8$ | O4 = −0.55 <br> O5 = −0.52 <br> O6 = −0.50 | O7 = −0.60 | O1 = −0.76 | O2 = −0.87 <br> O3 = −0.85 |

**Table 2** Charges computed for the titanium atoms in $Ti_{10}O_{12}(cat)_8(py)_8$, $Ti_{10}O_{12}(cat)_8(4\text{-Phpy})_8$, $Ti_{10}O_{12}(cat)_8(pico)_8$ and $Ti_{10}O_{12}(cat)_8(pyrald)_8$. $TiO_5N(bridging)$ refers to the titanium atoms coordinated by the catecholato ligands adopting the singly bridging $\mu^2\text{-}(O,O')$ mode

| | $TiO_5N(bridging)$ | $TiO_6$ | $TiO_5N$ |
|---|---|---|---|
| $Ti_{10}O_{12}(cat)_8(py)_8$ | Ti2 = +2.44 <br> $\langle q(Ti)\rangle$ = 2.11 ± 0.33 | Ti3 = +2.05 | Ti1 = +1.84 |
| $Ti_{10}O_{12}(cat)_8(4\text{-Phpy})_8$ | Ti1 = +2.45 <br> $\langle q(Ti)\rangle$ = 2.11 ± 0.34 | Ti2 = +2.05 | Ti3 = +1.85 |
| $Ti_{10}O_{12}(cat)_8(pico)_8$ | Ti1 = +2.42 <br> Ti10 = +2.44 <br> Ti3 = +2.44 <br> Ti5 = +2.45 <br> $\langle q(Ti)\rangle$ = 2.13 ± 0.32 | Ti8 = +2.04 <br> Ti6 = +2.05 | Ti9 = +1.86 <br> Ti4 = +1.86 <br> Ti7 = +1.87 <br> Ti2 = +1.87 |
| $Ti_{10}O_{12}(cat)_8(pyrald)_8$ | Ti2 = +2.45 <br> $\langle q(Ti)\rangle$ = 2.12 ± 0.33 | Ti3 = +2.08 | Ti1 = +1.84 |

$q$ = −0.50 to −0.61. Comparatively, the oxygen atoms, $\mu^2\text{-}O$ and $\mu^3\text{-}O$, forming the inorganic core of the complex are more negatively charged. Interestingly, the charges calculated for $\mu^2\text{-}O$ and $\mu^3\text{-}O$ are similar to those found in anatase or rutile $TiO_2$ ($q(O_{anatase})$ = −0.82 and $q(O_{rutile})$ = −0.81). The differences between the charges observed for titanium atoms in these structures are particularly pronounced as shown in Table 2. The charges for the titanium ions surrounded by 6 oxygens are around $q$ = +2.06 ± 0.02, whereas the titanium ions having a $TiO_5N$ coordination sphere and linked with the catecholato ligand adopting a bridging $\mu^2\text{-}(O,O')$ mode, display more positive charges between $q$ = +2.42 and $q$ = +2.45. These values contrast strongly with the partial charges computed for the titanium atoms inscribed in the second $TiO_5N$ subunit (these titanium atoms are coordinated by the catecholato ligands adopting the singly bridging chelate $\mu^2\text{-}(O,O',O')$ mode). These titanium atoms have less positive values around $q$ = +1.85 ± 0.02. Interestingly, charges of titanium inferior to $q$ = 2 are rather uncommon for neutral catecholato-based Titanium(IV) neutral complexes. According to the 13 structures of neutral

Ti(IV) complexes incorporating the catecholato ligand reported in the V1.1.1 webCSD release of the Cambridge Crystallographic Database, the charge of titanium ions are found superior to $q$ = +2 with a mean value of $q$ = +2.50 ± 0.34. A notable exception concerns a recently reported high nuclearity complex incorporating 17 titanium(IV) atoms. Here, the $q(Ti)$ values range from $q$ = +1.00 to +2.10.[10]

According to the charges calculated from these four structures, two categories of titanium could be distinguished. For the titanium atoms with $q(Ti)$ > 2, these atoms have charges compatible with titanium centers found in low nuclearity molecular complexes. The second category of titanium atoms ($q$ = +1.85 ± 0.02) resemble more to a titanium atom found in $TiO_2$ (anatase or rutile) $q(Ti)$ = 1.63.

## UV-visible spectroscopy

The UV-visible light absorption properties of the titanium oxoclusters were studied in solution ($CHCl_3$) and in the solid-
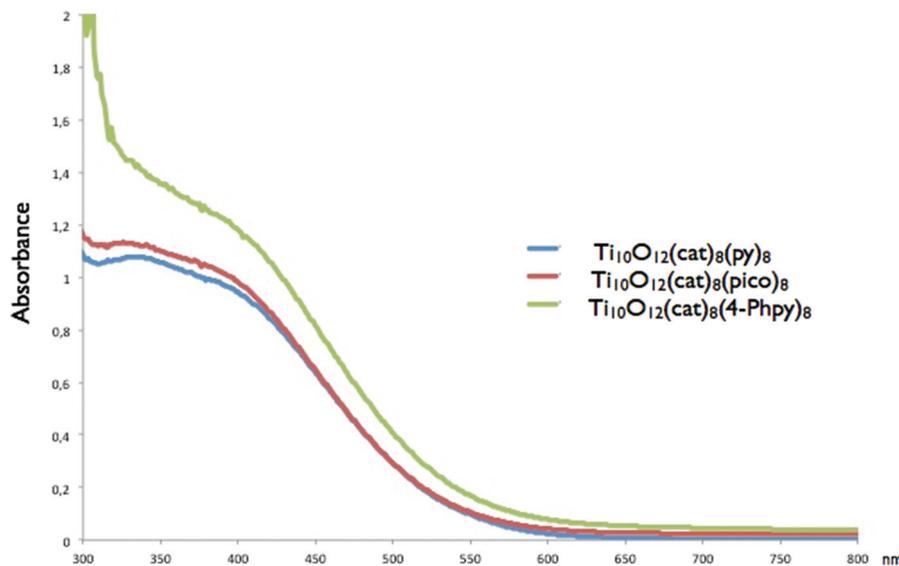
**Fig. 7** UV-visible spectra recorded for $Ti_{10}O_{12}(cat)_8(py)_8$ (blue curve), $Ti_{10}O_{12}(cat)_8(4\text{-Phpy})_8$ (green curve) and $Ti_{10}O_{12}(cat)_8(pico)_8$ (red curve) in chloroform ($c = 10^{-5}$ M).

state. The UV-visible absorption spectra of the complexes in solution were recorded only for $Ti_{10}O_{12}(cat)_8(py)_8$, $Ti_{10}O_{12}(cat)_8(4\text{-Phpy})_8$, and $Ti_{10}O_{12}(cat)_8(pico)_8$ ($c = 10^{-5}$ M) due to the insolubility of the $Ti_{10}O_{12}(cat)_8(pyrald)_8$ complex. These spectra are shown in Fig. 7. The spectra for the three complexes are rather similar. The complexes start to absorb light around 600 nm with a maximum in the visible region around 410 nm. In the UV domain, the complex bearing the 4-Phpy ligand absorbs strongly in comparison with its two analogues. Nevertheless, the nature of the pyridine ligands that substitute the oxo-clusters seems not to really affect the

absorption properties of visible light. These solid-state spectra are viewed in Fig. 8.

In the solid state, all species incorporating the $Ti_{10}O_{12}(cat)_8$ backbone display similar optical properties with a broad range of absorption in the visible domain between 400 nm and 650 nm. The band gaps are estimated for the five complexes using direct extrapolation of the absorption edges to the energy axis (see the ESI†). The $E_g$ values found for the different titanium-based species are compiled in Table 3. The band gaps for the complexes are rather similar ranging from 1.85 eV to 1.97 eV. Again, the nature of the nitrogen-ligands
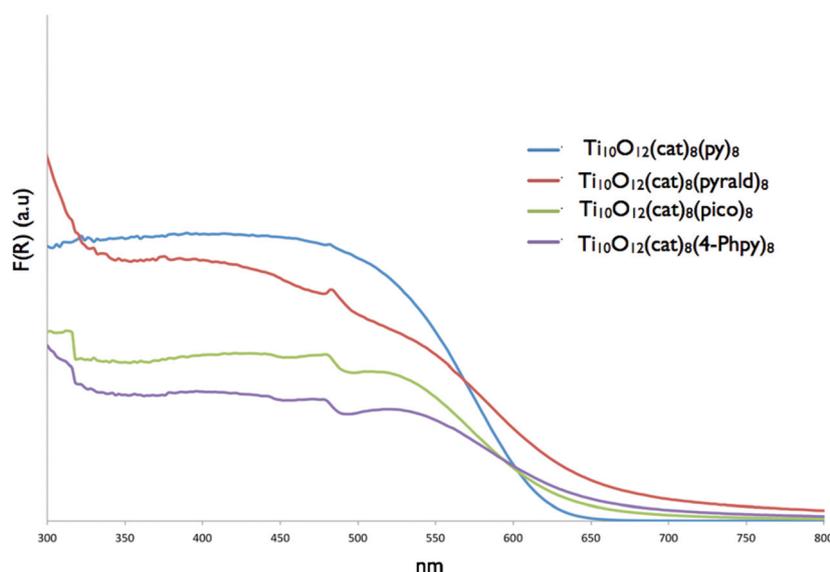


**Fig. 8** Solid-state optical diffuse-reflectance spectra of $Ti_{10}O_{12}(cat)_8(py)_8$ (blue curve), $Ti_{10}O_{12}(cat)_8(4\text{-Phpy})_8$ (purple curve), $Ti_{10}O_{12}(cat)_8(pico)_8$ (green curve), $Ti_{10}O_{12}(cat)_8(pyrald)_8$ (red curve) derived from diffuse reflectance data at room temperature. $F(R)$ is the Kubelka–Munk function.

**Table 3** The $E_g$ values obtained using the analysis of the adsorption edge

|  | $E_g$ values (eV) |
|---|---|
| $Ti_{10}O_{12}(cat)_8(py)_8$ | 1.97 |
| $Ti_{10}O_{12}(cat)_8(pico)_8$ | 1.88 |
| $Ti_{10}O_{12}(cat)_8(4\text{-}Phpy)_8$ | 1.86 |
| $Ti_{10}O_{12}(cat)_8(pyrald)_8$ | 1.85 |

seems not to significantly affect the solid-state electronic properties of the complexes. It should be noted that these band gaps estimated for our series of $Ti_{10}O_{12}(cat)_8$ structures are much lower compared to those found for $TiO_2$-based materials or nanoparticles or polyoxotitanate cages that ranges between 2.4 eV and 3.8 eV.[20]

## Theoretical calculations

Density functional theory (DFT) calculations on the $Ti_{10}O_{12}(cat)_8$ and $Ti_{10}O_{12}(cat)_8(py)_8$ have been performed with the Gaussian09 package,[21] using the hybrid exchange correlation functional B3LYP with a double-$\zeta$ basis function set with an ultrafine grid was used in all our calculations. This approach was chosen to be in line with previous theoretical studies reported on similar complexes.[22] For both complexes, geometry optimization started from the crystal structure geometry of $Ti_{10}O_{12}(cat)_8(py)_8$. In the case of $Ti_{10}O_{12}(cat)_8$, pyridine fragments were removed before calculation. The crystallographic symmetries were maintained in all of the calculations. GaussView was used for visualization of the computational results,[23] while DOS plots have been obtained with the GaussSum 2.2 software.[24] Even though the Kohn–Sham eigenstates should only be considered as a first approximation to one-particle energy levels and hence the obtained band gaps should therefore not be taken too literally, they are often informative in providing qualitative understanding of the electronic structures of materials and of the trend in band gaps.[6]

The HOMO, HOMO−1, HOMO−2 and LUMO, LUMO+1, LUMO+2 representations determined for $Ti_{10}O_{12}(cat)_8$ and $Ti_{10}O_{12}(cat)_8(py)_8$ are given in Fig. 9. For both complexes, the HOMO, HOMO−1 and HOMO−2 orbitals are localized exclusively on the catecholato ligands. Concerning the unoccupied orbitals (LUMO, LUMO+1, LUMO+2), they are originated almost exclusively from titanium d orbitals. Therefore, low energy transitions observed for the $Ti_{10}O_{12}(cat)_8(py)_8$ complex arise undoubtedly from catecholato-to-titanium charge transfer. Interestingly, the presence of the pyridine influences drastically the energy of the HOMO–LUMO gap. Energies of $\Delta E = -2.94$ eV and $\Delta E = -3.32$ eV are respectively found for $Ti_{10}O_{12}(cat)_8$ and $Ti_{10}O_{12}(cat)_8(py)_8$ (see Table 4). $Ti_{10}O_{12}(cat)_8$ has the lowest HOMO–LUMO gap calculated for a neutral catecholato-based titanium complex to date.[22] The density of states (DOS) plots for $Ti_{10}O_{12}(cat)_8$ and $Ti_{10}O_{12}(cat)_8(py)_8$ are reproduced in Fig. 10. These DOS plots evidence discrete energy levels for both complexes. However, we notice the influence of the pyridine ligands onto the $Ti_{10}O_{12}(cat)_8(py)_8$ DOS plots as the occupied levels are less energetically isolated compared to the occupied levels in $Ti_{10}O_{12}(cat)_8$.

## Conclusions

The post-synthetic modification of a catecholato polyoxotitanate nano-sized cluster has been demonstrated by taking advantage of the labile behavior of the pyridine ligands in $Ti_{10}O_{12}(cat)_8(py)_8$. Three $S_4$-symmetric complexes having an identical $Ti_{10}O_{12}(cat)_8$ backbone were isolated from $Ti_{10}O_{12}(cat)_8(py)_8$ and structurally characterized. These $Ti_{10}O_{12}(cat)_8$-based complexes incorporate two types of titanium atoms according the charge partial analysis: four Ti atoms in these structures display charges similar to those found in $TiO_2$ whereas the rest of the Ti atoms within these structures are related to Ti atoms found in molecular coordination compounds. These species strongly absorb light in the visible domain. According to DFT calculation, these strong absorbances are originated from HOMO–LUMO electronic transitions where the HOMOs are localized on the catecholato ligands and the LUMOs are centered on the d orbitals of titanium atoms. The DOS plots of $Ti_{10}O_{12}(cat)_8$ are far from displaying conduction and valence bands. Nevertheless, the pyridine ligands decorating the $Ti_{10}O_{12}(cat)_8$ backbone appear to impact the DOS plots towards the one expected for semiconductor nanoparticles. Overall, the $Ti_{10}O_{12}(cat)_8$ fragment appears to be an attractive building unit to generate Ti–O based hybrid materials absorbing visible light rather than ultraviolet light.[25]

## Experimental section

### General

All chemicals, solvents and reagents were of the best commercially available grade, purchased from Alfa Aesar, Sigma Aldrich and TCI Europe and used as received. $^1H$ and $^{13}C$ NMR spectra were recorded with a Bruker Avance 500 (500 MHz) spectrometer with the use of a deuterated solvent as the lock. The chemical shifts were expressed in parts per million (ppm, $\delta$) and referenced to residual solvent protons as internal standards ($^1H$ NMR: $CDCl_3$: $\delta = 7.26$ ppm, $CD_2Cl_2$: $\delta = 5.32$ ppm, DMSO: $\delta = 2.50$ ppm; $^{13}C$ NMR: $CDCl_3$: $\delta = 77.16$ ppm, $CD_2Cl_2$: $\delta = 53.84$ ppm, DMSO: $\delta = 39.52$ ppm). The description of signals include: s singlet, and dd doublet of doublets. The signal abbreviations include: Phenpyr-H (aromatic proton of 4-phenylpyridine), Pico-H (aromatic proton of 4-picoline), and Cat-H (aromatic proton of catechol). Infrared (IR) spectra were recorded with a Bruker Alpha FT-IR spectrometer. UV-Vis spectra were recorded with a BioTek UVIKON XL spectrometer. Thermogravimetric analyses (TGA) were performed on a Perkin-Elmer Pyris 6 TGA thermogravimetric analyser. Differential Scanning Calorimetry (DSC) spectra were obtained with a Perkin-Elmer Jade DSC calorimeter. Microanalyses were per-
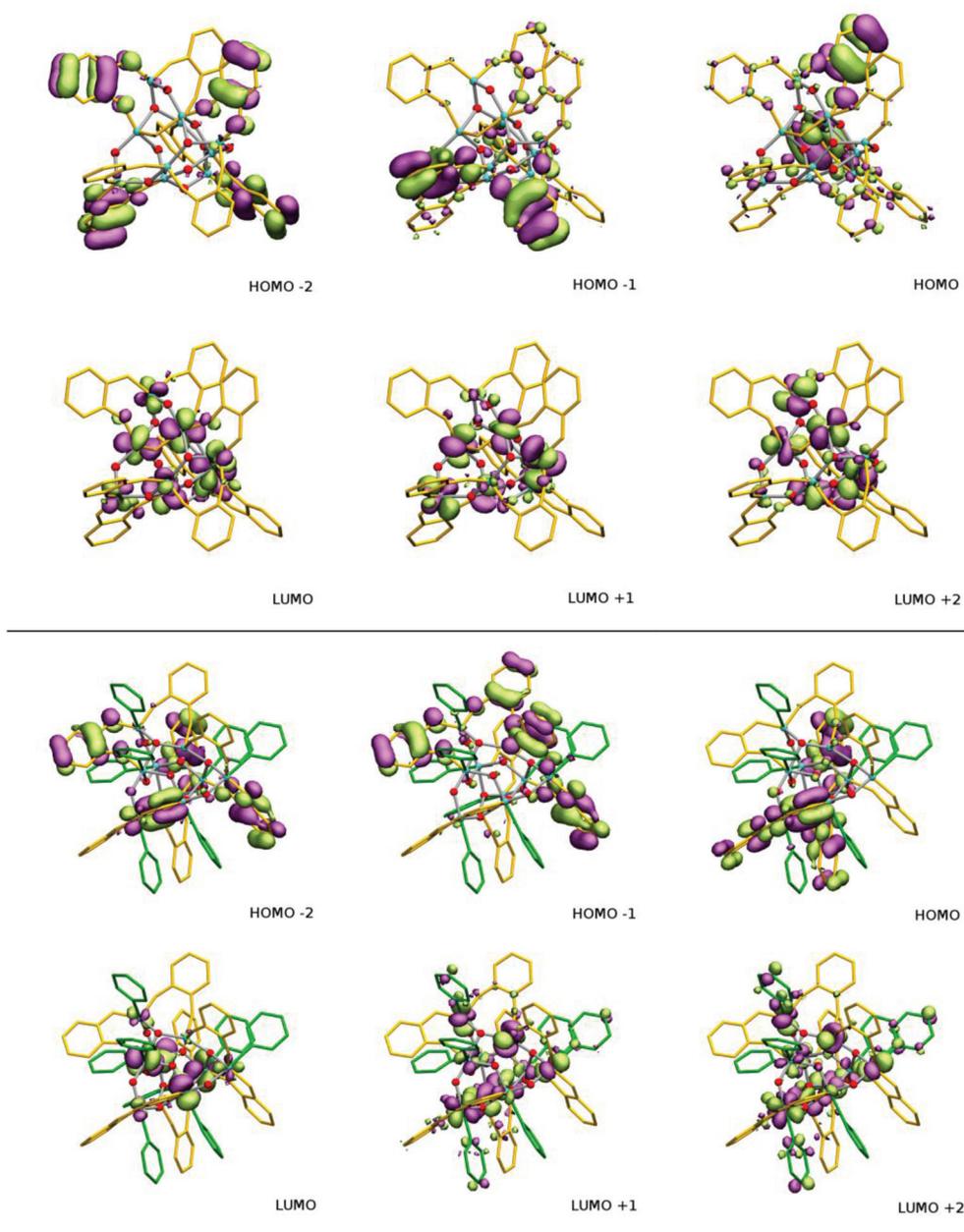
**Fig. 9** $Ti_{10}O_{12}(cat)_8$ (top) and $Ti_{10}O_{12}(cat)_8(py)_8$ (bottom): representation of the HOMO, HOMO−1 and HOMO−2 as well as the LUMO, LUMO+1 and LUMO+2 orbitals for both complexes. Catecholato ligands are represented in yellow, and pyridine ligands in green. Hydrogen atoms are omitted for clarity.

formed by the Service de Microanalyses de la Fédération de Recherche de Chimie, Université de Strasbourg, Strasbourg, France. Crystallography data were collected at 173(2) K with a Bruker APEX8 CCD diffractometer equipped with an Oxford Cryosystem liquid $N_2$ device, with the use of graphite-mono-chromated Mo-Kα ($\lambda$ = 0.71073 Å) radiation. For all structures, diffraction data were corrected for absorption and structural determination was achieved by using the APEX (1.022) package. $Ti_{10}O_{12}(cat)_8(pyr)_8$ was synthesized according to ref. 15.

**$Ti_{10}O_{12}(cat)_8(4\text{-Phpy})_8$.** The reaction was conducted under air. In a small glass vial, to a solution of $Ti_{10}O_{12}(cat)_8(py)_8$

(5 mg, 0.0023 mmol) dissolved in 0.750 mL of $CHCl_3$ was added a slight excess of 4-phenylpyridine (4-Phpy, 3 mg, 0.019 mmol) in 0.250 mL of $CHCl_3$. The reaction mixture was agitated for few seconds and set aside to crystallize by slow vapor diffusion of diethyl ether. Small dark red crystals were recovered by filtration and dried under vacuum during one night to afford $Ti_{10}O_{12}(cat)_8(4\text{-Phpy})_8$ in quantitative yield (6 mg). ^{1}H NMR (500 MHz, $CD_2Cl_2$): 8.40 (4-Phpy-H, broad s), 7.30 (4-Phpy-H, broad s), 7.22 (4-Phpy, broad s), 7.10 (Cat-H, broad, 4 H), 6.66 (Cat-H, complex, 8 H), 6.58 (Cat-H, broad, 8 H), 6.45 (Cat-H, complex, 4 H), 6.34 (Cat-H, complex, 4 H), 5.97

**Paper**

**Table 4** Calculated HOMO–LUMO gaps $\Delta E$ (eV) for $Ti_{10}O_{12}(cat)_8$ (top) and $Ti_{10}O_{12}(cat)_8(py)_8$

|  | $Ti_{10}O_{12}(cat)_8$ | $Ti_{10}O_{12}(cat)_8(py)_8$ |
|---|---|---|
| Symmetry | $S_4$ | $S_4$ |
| $E_{LUMO}$ | −3.26 | −1.85 |
| $E_{HOMO}$ | −6.20 | −5.17 |
| $\Delta E$ | −2.94 | −3.32 |
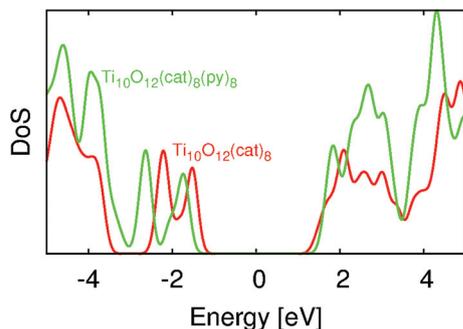


**Fig. 10** DOS plots of the $Ti_{10}O_{12}(cat)_8$ (red) and $Ti_{10}O_{12}(cat)_8(py)_8$ (green) complexes.

(Cat-H, complex, 4 H) ppm. $^{13}C$ NMR (125 MHz, $CD_2Cl_2$): 159.5 (C–O catecholato), 157.7 (C–O catecholato), 156.1 (C–O catecholato), 154.2 (C–O catecholato), 150.1 (C–H (2,6)phenylpyridine), 149.1 (C (4)phenylpyridine), 137.6 (C (7)phenylpyridine), 129.9 (C–H (10)phenylpyridine), 129.4 (C–H (9,11)phenylpyridine), 127.3 (C–H (8,12)phenylpyridine), 121.8 (C–H (3,5)phenylpyridine), 121.3 (C–H catecholato), 120.9 (C–H catecholato), 120.4 (C–H catecholato), 120.1 (C–H catecholato), 119.9 (C–H catecholato), 118.0 (C–H catecholato), 115.5 (C–H catecholato), 112.5 (C–H catecholato) ppm. IR: 1614, 1477, 1255, 1212, 1100, 1018, 881, 744, 698, 628, 504, 440 cm$^{-1}$. Anal. calcd for $C_{136}H_{104}N_8O_{28}Ti_{10}\cdot CHCl_3$: C 56.81; H 3.65; N 3.87. Found C 56.37; H 4.05; N 4.00. X-ray data: empirical formula: $C_{140}H_{108}Cl_{12}N_8O_{28}Ti_{10}$ ($C_{136}H_{104}N_8O_{28}Ti_{10}$, 4($CHCl_3$)); formula mass: 3254.74; crystal system: tetragonal; space group: $I4_1/a$; unit cell dimensions: $a = 29.1802(10)$ Å, $b = 29.1802(10)$ Å, $c = 16.1450(6)$ Å; $V = 13\,747.2(8)$ Å$^3$; $Z = 4$; density (calcd): 1.573 mg m$^{-3}$; crystal size: $0.06 \times 0.03 \times 0.03$ mm$^3$; $\theta$ range for data collection: 1.40–30.05°; reflections collected: 51 412; independent reflections: 9678 [$R$(int) = 0.0991]; refinement method: full-matrix least squares on $F^2$; data/restraints/parameters: 9678/0/447; goodness-of-fit on $F^2$: 1.005; final $R$ indices [$I > 2\sigma(I)$]: $R_1 = 0.0829$, w$R_2 = 0.1402$; $R$ indices (all data): $R_1 = 0.1803$, w$R_2 = 0.2206$. CCDC 1413510.

**$Ti_{10}O_{12}(cat)_8(pyrald)_8$.** A similar procedure as the one described just above was used by replacing 4-phenylpyridine with 2-methoxy-5-(pyridin-4-yl)benzaldehyde (pyrald). Small dark red crystals (7 mg) were recovered in quantitative yield by filtration and dried under vacuum. IR: 2950, 1734, 1681, 1604, 1579, 1475, 1426, 1389, 1273, 1251, 1212, 1177, 1124, 1100, 1069, 1053, 1012, 906, 810, 744, 673, 502, 473, 428 cm$^{-1}$. Anal. calcd for $C_{152}H_{120}N_8O_{44}Ti_{10}\cdot 3CHCl_3$: C 51.72; H 3.44; N 3.11. Found C 51.68; H 3.57; N 3.19. X-ray data: empirical formula: $C_{156}H_{124}Cl_{12}N_8O_{44}Ti_{10}$ ($C_{152}H_{120}N_8O_{44}Ti_{10}$, 4($CHCl_3$)); formula mass: 3719.03; crystal system: tetragonal; space group: $I4_1/a$; unit cell dimensions: $a = 31.272(3)$ Å, $b = 31.272(3)$ Å, $c = 15.6882(14)$ Å; $V = 15\,342(2)$ Å$^3$; $Z = 4$; density (calcd): 1.610 mg m$^{-3}$; crystal size: $0.05 \times 0.04 \times 0.04$ mm$^3$; $\theta$ range for data collection: 2.61–27.55°; reflections collected: 33 930; independent reflections: 8798 [$R$(int) = 0.0699]; refinement method: full-matrix least squares on $F^2$; data/restraints/parameters: 8798/0/521; goodness-of-fit on $F^2$: 1.054; final $R$ indices [$I > 2\sigma(I)$]: $R_1 = 0.1172$, w$R_2 = 0.2389$; $R$ indices (all data): $R_1 = 0.2592$, w$R_2 = 0.3086$. CCDC 1413511.

**$Ti_{10}O_{12}(cat)_8(pico)_8$.** A similar procedure as the one described just above was used by replacing 2-methoxy-5-(pyridin-4-yl)benzaldehyde with 4-picoline (pico). Small dark red crystals (5 mg) were quantitatively recovered by filtration and dried under vacuum. $^1H$ NMR (500 MHz, $CD_2Cl_2$): 8.11 (Pico-H, broad s), 7.13 (Cat-H, dd, $^3J = 7.6$ Hz, $^4J = 1.2$ Hz, 4 H), 6.63 (Cat-H, complex, 8 H), 6.51 (Cat-H, complex, 4 H), 6.46 (Cat-H, complex, 4 H), 6.41 (Cat-H, complex, 4 H), 6.34 (Cat-H, complex, 4 H), 6.17 (Pico-H, broad s), 5.94 (Cat-H, dd, $^3J = 7.6$ Hz, $^4J = 1.1$ Hz, 4 H) ppm. $^{13}C$ NMR (125 MHz, $CD_2Cl_2$): 159.4 (C–O catecholato), 157.5 (C–O catecholato), 155.9 (C–O catecholato), 154.1 (C–O catecholato), 149.9 (C–H (2,6)picoline), 148.2 (C (4)picoline), 124.5 (C–H (3,5)picoline), 120.3 (C–H catecholato), 120.2 (C–H catecholato), 120.1 (C–H catecholato), 120.0 (C–H catecholato), 119.8 (C–H catecholato), 117.9 (C–H catecholato), 115.4 (C–H catecholato), 112.3 (C–H catecholato), 21.0 (CH$_3$ picoline) ppm. IR: 3065, 1618, 1575, 1473, 1438, 1291, 1253, 1212, 1100, 1018, 900, 818, 773, 740, 675, 663, 624, 589, 540, 514, 489, 430 cm$^{-1}$. Anal. calcd for $C_{96}H_{88}N_8O_{28}Ti_{10}\cdot CHCl_3$: C 48.55; H 3.74; N 4.67. Found C 48.50; H 3.85; N 4.66. X-ray data: empirical formula: $C_{100}H_{92}Cl_{12}N_8O_{28}Ti_{10}$ ($C_{96}H_{88}N_8O_{28}Ti_{10}$, 4($CHCl_3$)); formula mass: 2758.22; crystal system: triclinic; space group: $P\bar{1}$; unit cell dimensions: $a = 15.6659(9)$ Å, $b = 18.9579(11)$ Å, $c = 23.2236(13)$ Å; $V = 6191.9(6)$ Å$^3$; $Z = 2$; density (calcd): 1.479 mg m$^{-3}$; crystal size: $0.07 \times 0.06 \times 0.05$ mm$^3$; $\theta$ range for data collection: 1.16–27.21°; reflections collected: 26 308; independent reflections: 26 308 [$R$(int) = 0.0541]; refinement method: full-matrix least squares on $F^2$; data/restraints/parameters: 26 308/0/1431; goodness-of-fit on $F^2$: 1.005; final $R$ indices [$I > 2\sigma(I)$]: $R_1 = 0.0720$, w$R_2 = 0.1603$; $R$ indices (all data): $R_1 = 0.1540$, w$R_2 = 0.1802$. CCDC 1413512.

## Acknowledgements

# References

1  A. Fujishima and K. Honda, *Nature*, 1972, **238**, 37.

2  (*a*) A. L. Linsebigler, G. Lu and J. T. Yates, *Chem. Rev.*, 2009, **109**, 735; (*b*) S. Josset, N. Keller, M.-C. Lett and V. Keller, *Chem. Soc. Rev.*, 2008, **37**, 744.

3  M. Gratzel, *Inorg. Chem.*, 2005, **44**, 6841.

4  L. Rozes and C. Sanchez, *Chem. Soc. Rev.*, 2011, 1006.

5  S. Eslava, M. McPartlin, R. I. Thomson, J. M. Rawson and D. S. Wright, *Inorg. Chem.*, 2010, **49**, 11532.

6  Y. Lv, J. Cheng, P. D. Matthews, J. P. Holgado, J. Willkomm, M. Leskes, A. Steiner, D. Fenske, T. C. King, P. T. Wood, L. Gan, R. M. Lambert and D. S. Wright, *Dalton Trans.*, 2014, **43**, 8679.

7  Y. Lv, J. Cheng, A. Steiner, L. Gan and D. S. Wright, *Angew. Chem., Int. Ed.*, 2014, **53**, 1934.

8  (*a*) Y. Chen, J. D. Sokolow, E. Trzop and P. Coppens, *Dalton Trans.*, 2013, **42**, 15285; (*b*) Y. Chen, J. Sokolow, E. Trzop, Y.-S. Chen and P. J. Coppens, *J. Chin. Chem. Soc.*, 2013, **60**, 887; (*c*) S. Eslava, B. P. R. Goodwill, M. McPartlin and D. S. Wright, *Inorg. Chem.*, 2011, **50**, 5655.

9  Y. Lv, J. Willkomm, M. Leskes, A. Steiner, T. C. King, L. Gan, E. Reisner, P. T. Wood and D. S. Wright, *Chem. – Eur. J.*, 2012, **18**, 11867.

10  Y. Chen, E. Trzop, A. Makal, J. D. Sokolow and P. Coppens, *Inorg. Chem.*, 2013, **52**, 4750.

11  (*a*) J.-X. Yin, P. Huo, S. Wang, J. Wu, Q.-Y. Zhu and J. Dai, *J. Mater. Chem. C*, 2015, **3**, 409; (*b*) Y.-Y. Wu, P. Wang, Y.-H. Wang, J.-B. Jiang, G.-Q. Bian, Q.-Y. Zhu and J. Dai, *J. Mater. Chem. A*, 2013, **1**, 9862; (*c*) J. D. Sokolow, E. Trzop, Y. Chen, J. Tang, L. J. Allen, R. H. Crabtree, J. B. Benedict and P. Coppens, *J. Am. Chem. Soc.*, 2012, **134**, 11695; (*d*) J. B. Benedict and P. Coppens, *J. Am. Chem. Soc.*, 2010, **132**, 2938.

12  (*a*) T. J. Boyle, L. J. Tribby, T. M. Alam, S. D. Bunge and G. P. Holland, *Polyhedron*, 2005, **24**, 1143; (*b*) K. Gigant, A. Rammal and M. Henry, *J. Am. Chem. Soc.*, 2001, **123**, 11632.

13  J. P. Corden, W. Errington, P. Moore, M. G. Partrige and M. G. H. Wallbridge, *Dalton Trans.*, 2004, 1846.

14  H. Senouci, B. Millet, C. Volkringer, C. Huguenard, F. Taulelle and M. Henry, *C. R. Chim.*, 2010, **13**, 69.

15  C. Chaumont, P. Mobian and M. Henry, *Dalton Trans.*, 2014, **43**, 3416.

16  (*a*) C. Chaumont, E. Huen, C. Huguenard, P. Mobian and M. Henry, *Polyhedron*, 2013, **57**, 70; (*b*) G. Soler-Illia, L. Rozes, M. K. Boggiano, C. Sanchez, C. O. Turrin, A. M. Caminade and J. P. Majoral, *Angew. Chem., Int. Ed.*, 2000, **39**, 4250.

17  (*a*) T. Frot, S. Cochet, G. Laurent, C. Sassoye, M. Popall, C. Sanchez and L. Rozes, *Eur. J. Inorg. Chem.*, 2010, 5650;

(*b*) I. Mijatovia, G. Kickelbick, M. Puchberger and U. Schubert, *New J. Chem.*, 2003, **27**, 3.

18  S. Kim, W. Hwang, I. S. Lim, S. H. Kim, S.-G. Lee and B. M. Kim, *Tetrahedron Lett.*, 2010, **51**, 709.

19  (*a*) M. Henry, *ChemPhysChem*, 2002, **3**, 561; (*b*) M. Henry, *ChemPhysChem*, 2002, **3**, 607; (*c*) M. Henry and M. W. Hosseini, *New J. Chem.*, 2004, **28**, 897; (*d*) C. Carpanese, S. Ferlay, N. Kyritsakas, M. Henry and M. W. Hosseini, *Chem. Commun.*, 2009, 6786; (*e*) M. Henry, in *Advances in Quantum Chemical Bonding Structures*, ed. M. V. Putz, Transworld Research Network, Kerala, India, 2009, pp. 153–211; (*f*) H. Senouci, B. Millet, C. Volkringer, C. Huguenard, F. Taulelle and M. Henry, *C. R. Chim.*, 2010, **13**, 69; (*g*) M. Henry, in *Encyclopedia of Nanoscience and Nanotechnology*, ed. H. S. Nalwa, American Scientific Publishers, 2011, vol. 14, pp. 1–43.

20  P. D. Matthews, T. C. King and D. S. Wright, *Chem. Commun.*, 2014, **50**, 12815.

21  M. J. Frisch, G. W. Trucks, H. B. Schlegel, G. E. Scuseria, M. A. Robb, J. R. Cheeseman, G. Scalmani, V. Barone, B. Mennucci, G. A. Petersson, H. Nakatsuji, M. Caricato, X. Li, H. P. Hratchian, A. F. Izmaylov, J. Bloino, G. Zheng, J. L. Sonnenberg, M. Hada, M. Ehara, K. Toyota, R. Fukuda, J. Hasegawa, M. Ishida, T. Nakajima, Y. Honda, O. Kitao, H. Nakai, T. Vreven, J. A. Montgomery Jr., J. E. Peralta, F. Ogliaro, M. Bearpark, J. J. Heyd, E. Brothers, K. N. Kudin, V. N. Staroverov, R. Kobayashi, J. Normand, K. Raghavachari, A. Rendell, J. C. Burant, S. S. Iyengar, J. Tomasi, M. Cossi, N. Rega, J. M. Millam, M. Klene, J. E. Knox, J. B. Cross, V. Bakken, C. Adamo, J. Jaramillo, R. Gomperts, R. E. Stratmann, O. Yazyev, A. J. Austin, R. Cammi, C. Pomelli, J. W. Ochterski, R. L. Martin, K. Morokuma, V. G. Zakrzewski, G. A. Voth, P. Salvador, J. J. Dannenberg, S. Dapprich, A. D. Daniels, Ö. Farkas, J. B. Foresman, J. V. Ortiz, J. Cioslowski and D. J. Fox, *Gaussian 09, Revision D.01*, Gaussian, Inc., Wallingford, CT, 2009.

22  J. B. Benedict and P. Coppens, *J. Am. Chem. Soc.*, 2010, **132**, 2936.

23  R. Dennington, T. Keith and J. Millam, *GaussView, Version 5*, Semichem Inc., Shawnee Mission, KS, 2009.

24  N. M. O'Boyle, A. L. Tenderholt and K. M. Langner, *J. Comput. Chem.*, 2008, **29**, 839.

25  (*a*) M. Dan-Hardi, C. Serre, T. Frot, L. Rozes, G. Maurin, C. Sanchez and G. Férey, *J. Am. Chem. Soc.*, 2009, **131**, 10857; (*b*) C. H. Hendon, D. Tiana, M. Fontecave, C. Sanchez, L. D'arras, C. Sassoye, L. Rozes, C. Mellot-Draznieks and A. Walsh, *J. Am. Chem. Soc.*, 2013, **135**, 10942.